

Turbulent flow field comparison and related suitability for fish passage of a standard and a simplified low-gradient vertical slot fishway

*Original*

Turbulent flow field comparison and related suitability for fish passage of a standard and a simplified low-gradient vertical slot fishway / Quaranta, Emanuele; Katopodis, Christos; Revelli, Roberto; Comoglio, Claudio. - In: RIVER RESEARCH AND APPLICATIONS. - ISSN 1535-1459. - STAMPA. - (2017), pp. 1-11. [10.1002/rra.3193]

*Availability:*

This version is available at: 11583/2678527 since: 2017-08-25T12:02:14Z

*Publisher:*

Wiley Online Library

*Published*

DOI:10.1002/rra.3193

*Terms of use:*

This article is made available under terms and conditions as specified in the corresponding bibliographic description in the repository

*Publisher copyright*

(Article begins on next page)

# Turbulent flow field comparison and related suitability for fish passage of a standard and a simplified low-gradient vertical slot fishway

Numerical simulations of vertical slot fishways

Quaranta E.<sup>1</sup>, Katopodis C<sup>2</sup>., Revelli R<sup>3</sup>., Comoglio C.<sup>4</sup>

<sup>1 4</sup>, *Politecnico di Torino, DIATI (Department of Environment, Land and  
Infrastructure Engineering).*

*Corso Duca degli Abruzzi 24, 10129, Torino, Italia*

<sup>3</sup>, *Politecnico di Torino, DIATI and Duke University (USA).*

<sup>2</sup> *Katopodis Ecohydraulics Ltd., Winnipeg, Canada*

---

## Abstract

1 Fishways are hydraulic structures that allow passage of fish across ob-  
2 structions in rivers. Vertical slot fishways -VSF- are considered the most  
3 efficient and least selective type of technical fishway solutions, especially due  
4 to their ability to remain effective even when significant upstream and/or  
5 downstream water level fluctuations occur. The scope of the present study  
6 is to perform numerical simulations in order to investigate and compare  
7 the hydraulic turbulent flow field in a standard and a simplified version of  
8 the most common VSF design. Implications in relation to fish swimming  
9 behavior and fish passage performance are discussed.

---

\*<sup>1</sup>(corresponding author). emanuele.quaranta@polito.it, Tel: 0039 0110905682

\*\*<sup>2</sup>KatopodisEcohydraulics@live.ca

<sup>3</sup>roberto.revelli@polito.it

<sup>4</sup> claudio.comoglio@polito.it

10 Different water depths (as well as discharges) were investigated, using  
11 a bed slope of 5%, as a reference for low-gradient VSFs with a very lim-  
12 ited selectivity that can be used in multispecies rivers in grayling-barbel  
13 regions. Results show that maximum values of velocity, turbulent kinetic  
14 energy and Reynolds stresses are higher in the standard design. However,  
15 corresponding to slot geometry and orientation, the direction of the main  
16 jet in the simplified design is more inclined towards the left side of the  
17 pool. This causes the eddy to split into two smaller ones; the minimum  
18 eddy dimension is reduced from 0.4-0.5 m to 0.2-0.3 m. These dimensions  
19 are detrimental for fish passage efficiency, being more comparable with fish  
20 length (0.15-0.40 m), thus affecting migrating fish stability and orientation.  
21 Furthermore, the standard design provides a more straightforward upstream  
22 path and wider areas of low flow velocities and turbulence, useful for fish  
23 resting. Therefore, it is recommended that the standard design should be  
24 preferred over its simplified version, even if its construction costs are around  
25 10-15% higher than the simplified one.

*Keywords:* CFD, ecohydraulics, fish passage, fishway, vertical slot fishway

---

## 1. Introduction

26 Throughout the world, anthropogenic obstructions in rivers have gener-  
27 ated relevant adverse effects on fish migratory routes. The interruption of  
28 longitudinal connectivity of a natural river is perceived as one of the main  
29 causes in the decline of freshwater ichthyofauna (Calles and Greenberg,  
30 2009).

31 In order to restore to an acceptable level the longitudinal connectivity

32 of a river fragmented by man-made obstacles, the construction of effective  
33 fishways represents the best practice where obstacle removal is not feasible.  
34 Fishways are hydraulic structures designed to allow passage of upstream  
35 migrating fish through river obstructions, such as weirs or dams. Pool-type  
36 are the most common fishway used worldwide (Bunt et al., 2012; Hatry et  
37 al., 2013; Santos et al., 2012). Pool-type fishways consist of a channel with  
38 a sloping bed that is divided into a series of pools by cross-walls at regular  
39 intervals.

40 Different fishway geometries lead to different hydraulic flow fields, and,  
41 as a consequence, a certain typology will likely be more suitable for some  
42 species and fish lengths, and less for others. Hence the design of a fishway  
43 has to take into account the swimming capability, size and behavior of the  
44 species of concern (Clay, 1995; Katopodis and Williams, 2012; Katopodis  
45 and Gervais, 2016).

#### 46 *1.1. Fish and flow field interaction*

47 The flow field in a fishway affects species behavior, and the capability  
48 of fish to successfully migrate through it. Indeed, the flow field generates  
49 shear stresses and hydrodynamic resistance on fish, making migration an  
50 energetically demanding process. Hence fishway design needs to be based  
51 on biological characteristics of the fish species that are expected to migrate  
52 upstream of the considered obstacle, with particular regard to their mor-  
53 phology, behavior and swimming ability. Maximum allowed flow velocity  
54 value (occurring in the slot) is defined based on the burst speed of the  
55 weakest fish species expected to migrate. Together with body size of the  
56 largest migrants, it constitutes a significant parameter affecting fishway di-

57 mensions and related construction costs (mainly related to bottom slope  
58 and pool dimensions).

59 When passing from one pool to the upstream one, fish can reach burst  
60 speed; this is the top speed, which lasts for a few seconds, by the exclusive  
61 utilization of white muscles (Plaut, 2001). Flow velocity creates hydro-  
62 dynamic resistance to fish, and when it exceeds burst speed, migration  
63 can be seriously compromised. Therefore, the maximum upstream migra-  
64 tion distance diminishes as flow velocity increases (Katopodis and Gervais,  
65 2016). For example, it is estimated that distance traveled by cyprinids and  
66 salmonids decreases for flow velocities higher than 1.5 m/s, that are typical  
67 velocities encountered by fish when passing from one pool to the next one  
68 (Puertas et al., 2012). Hence fish need resting areas, characterized by lower  
69 flow velocities (e.g. velocities of 0.2-0.4 m/s are recommended values for  
70 cyprinids-Iberian barbel), for a short resting before a subsequent upstream  
71 movement through higher velocity areas (Silva et al., 2011).

72 Also turbulence affects fish behavior. The most relevant turbulent vari-  
73 ables are turbulent kinetic energy ( $TKE$ ), eddies diameter and Reynolds  
74 stresses ( $RS$ ) (Silva et al. 2012; Silva et al., 2015).

75  $TKE$  (kinetic energy associated with fluctuating components of the ve-  
76 locity) affects fish swimming performance by increasing swimming costs.  
77 High  $TKE$  can confuse fish in their efforts to move though the fishway  
78 along energy efficient paths, increasing fish fatigue. Silva et al. (2011) have  
79 noticed that Iberian barbel used low  $TKE$  locations ( $TKE \leq 0.05 \text{ m}^2/\text{s}^2$ ) as  
80 resting areas before subsequent efforts to traverse areas of higher velocity  
81 and turbulence (i.e. along the main jet). Therefore, a large portion of the

82 pool should stay below  $TKE \leq 0.05 \text{ m}^2/\text{s}^2$ . This means that in low velocity  
83 areas also low  $TKE$  values should be provided.

84 Shear stresses and Reynolds stresses  $RS$  ( $RS$  are shear stresses gener-  
85 ated by fluctuations in velocity over time due to turbulence, while shear  
86 stresses are generated by fluid viscosity) affect fish swimming performance  
87 and stability, and can even cause injury or mortality (Silva et al., 2011; Silva  
88 et al., 2012; Silva et al., 2015). In Silva et al. (2011), it has been observed  
89 that on the horizontal plane barbel occupied positions with absolute  $RS$   
90  $\leq 60 \text{ N/m}^2$ . Thus  $RS \leq 60 \text{ N/m}^2$  can be considered a reference threshold.

91 Furthermore, the diameter of eddies forming in the fishway flow plays an  
92 important role. The interaction with eddies is a complex phenomenon that  
93 results from the capacity of fish to integrate biomechanics, physiological and  
94 sensory processes (Marriner et al., 2016). If eddies are significantly smaller  
95 than fish size, fish may swim steadily through them. Eddy diameters close  
96 to the length of migrating fish, particularly in combination with high eddy  
97 vorticity, can affect fish stability and result in reduced fishway performance.  
98 When eddy size is larger than fish total length, fish orientation disturbance  
99 is minimal (Silva et al., 2012; Tritico and Cotel, 2010).

100 Therefore, based on the aforementioned scientific literature, it is recom-  
101 mended that resting zones with  $TKE \leq 0.05 \text{ m}^2/\text{s}^2$  and  $RS \leq 60 \text{ N/m}^2$   
102 be provided in 30% to 50% of the pool, with velocities kept under 0.30  
103 m/s, keeping eddies dimensions to adequate values compared to upstream  
104 migrants body lengths.

105 *1.2. Vertical slot fishways*

106 Vertical slot fishways -VSF- are considered the most efficient and least  
107 selective type of technical fish pass solutions, especially due to their abil-  
108 ity to remain effective even when significant upstream and/or downstream  
109 water level fluctuations occur. The velocity field in the pools is relatively in-  
110 sensitive to flow rate variations (Katopodis, 1992). VSF are recommended  
111 especially in rivers where several fish species with different swimming ca-  
112 pabilities are present (FAO and DVWK, 2002). VSFs basically consist of  
113 a sloping rectangular channel divided into a number of pools by vertical  
114 baffles. Water flows through the vertical slot between the baffles, from one  
115 pool to the downstream one. The water level difference between two ad-  
116 jacent pools depends on the slope of the fishway and on the length of the  
117 pool.

118 Rajaratnam et al. (1992) evaluated eighteen different designs of VSF  
119 using physical models. In particular, Design 1 is the most common design (a  
120 standard reference commonly used in real applications), while Design 16 is  
121 its simplified version, and it represents a low cost option for the construction  
122 of a VSF (see Fig.1). The slot orientation, i.e. the angle between the width  
123 of the slot and the longitudinal direction, is  $\alpha = 45^\circ$  for Design 1 and  
124  $\alpha = 34^\circ$  for Design 16. The two designs differ also on the shape of the  
125 baffles, as it can be seen in Fig.1. The baffle shape of Design 1 is more  
126 complex, leading to higher construction costs.

127 Conventionally, analysis of VSFs hydrodynamics and their design have  
128 been performed using physical models (Rajaratnam et al., 1992; Wu et  
129 al., 1999; Puertas et al., 2004), whereas field experiments have been con-

130 ducted for evaluating fish passage efficiencies (Laine et al., 1998; Stuart  
131 and Berghuis, 2002). In recent decades, improvements in computer technol-  
132 ogy and numerical algorithms, have allowed computational fluid dynamics  
133 (CFD) to be increasingly used for hydraulic problems, including fishways.  
134 For example, in Khan (2006) and Marriner et al. (2014), 3D CFD simula-  
135 tions of VSF have been performed, solving the 3D RANS (Reynolds Average  
136 Navier Stokes) equations.

137 The scope of the present work is to show a detailed comparison and flow  
138 field description of the two vertical slot fishway designs. The main objective  
139 is to understand through the use CFD tools, if the simplified design, whose  
140 construction costs are generally 10-15% lower (based on personal commu-  
141 nications about cost estimates collected from four construction firms), can  
142 have the same effectiveness as the standard one.

143 Model results for the two designs were compared with reference to rep-  
144 resentative turbulent flow field parameters (e.g.  $TKE$ ,  $RS$ , see section 1.1)  
145 identified as the most influential on fish passage by the latest experimental  
146 studies. Furthermore, the 3D modeling was carried out with the aim of  
147 analyzing possible changes in the turbulent flow field generated at varying  
148 depths along the two typologies of VSF.

## 149 **2. Method**

### 150 *2.1. Geometry*

151 The geometric design of the two typologies of VSF is depicted in Fig.1,  
152 using a slot width  $b_0 = 0.30$  m. The length and width of the pool are  
153  $L = 10b_0$  and  $b = 8b_0$ , respectively; these are established across North

154 America and Europe as the recommended design dimensions for regular  
155 pools (Marriner et al., 2016). These correspond to a pool length of 3 m and  
156 a pool width of 2.4 m.

157 In order to find an optimal compromise between accuracy and compu-  
158 tational cost, five pools were simulated (pools were named pool 2-3-4-5-6  
159 from upstream to downstream), with a 6 m long headrace (pool 1) and a 6  
160 m long tailrace (pool 7), where inlet/outlet boundary conditions were im-  
161 posed, respectively. Results are discussed in relation to pool 4 which is used  
162 as a reference for a typical pool. In pool 4 the flow field can be considered  
163 the representative one, also for a VSF with a bigger number of pools (as  
164 confirmed in Khan, 2006; Heimerl et al., 2008).

165 The adopted bed slope is 5%, which is considered an appropriate value  
166 for multispecies rivers to limit species selectivity (Katopodis and Williams,  
167 2012; Schmutz and Mielach, 2013). Therefore, the analyzed VSF is con-  
168 sidered as a low-gradient fishway by international standards (White et al.,  
169 2011). Considering a pool length of 3 m, the head drop between two pools  
170 is 0.15 m, which is a suitable value for a wide variety of fish species in  
171 barbel-grayling regions, including large migrants such as Danube salmon  
172 and Northern pike (Schmutz and Mielach, 2013).

## 173 *2.2. Hydraulic conditions*

174 Considering the relationship linking the water depth at the center of the  
175 pool  $y_0$  with the flow rate (Rajaratnam et al., 1992), flow rates correspond-  
176 ing to values  $y_0 = 1$  m,  $y_0 = 1.5$  m and  $y_0 = 2$  m were used to investigate  
177 possible changes of the turbulent flow field at varying water depths (as well  
178 as flow rates). Using three different values of  $y_0$  means that, for each design,

179 three different flow rate conditions were simulated. Using the bed slope of  
180 5%, and the equations reported in Rajaratnam et al. (1992), flow rates were  
181  $Q = 0.395 \text{ m}^3/\text{s}$ ,  $Q = 0.612 \text{ m}^3/\text{s}$  and  $Q = 0.829 \text{ m}^3/\text{s}$  for Design 1, and  
182  $Q = 0.413 \text{ m}^3/\text{s}$ ,  $Q = 0.619 \text{ m}^3/\text{s}$  and  $Q = 0.826 \text{ m}^3/\text{s}$  for Design 16. The  
183 generated flow rates are similar for the two designs, with slight differences  
184 due to the dissimilar flow field generated by the altered geometry.

185 Following the approach reported in Khan (2006), planes parallel to the  
186 bed were used for the description of the flow field. In Khan (2006), the  
187 following planes were used: the deepest ones were  $H_1$  at  $y/y_0 = 0.05$  and  
188  $H_2$  at  $y/y_0 = 0.33$  (these represent the flow field for bottom oriented fish  
189 species). In contrast, planes  $H_4$  at  $y/y_0 = 0.67$  and  $H_5$  at  $y/y_0 = 0.95$   
190 represent the flow field faced by fish swimming in the upper portion of  
191 the water column. The last plane is  $H_3$  at  $y/y_0 = 0.5$ . The components  
192 of velocity normal to these planes were negligible, as shown in Wu et al.  
193 (1999): this is an expected result for bed slopes lower than 10%.

### 194 *2.3. Mesh*

195 A tetrahedral computational mesh was generated, which becomes hex-  
196 ahedral when approaching the bed. The mesh cell dimensions ranged from  
197 0.025 m at the walls to 0.05 m in the pools. These values are comparable  
198 and finer with respect to those adopted in Khan (2006) -0.025 to 0.100 m-,  
199 and in Marriner et al. (2014) -0.11 m-. Considering the dimensions of the  
200 hydraulic flow field structure typical of such fishways (e.g. eddies), these  
201 cell dimensions can be considered adequate for simulating the flow field  
202 affecting fish behavior.

203 *2.4. CFD model: setup*

204 Reynolds Averaged Navier–Stokes (RANS) equations were solved by  
 205 the software FLUENT to simulate the average flow field. Three momentum  
 206 equations (one equation for each cartesian coordinate) and the continuity  
 207 equation were solved. The VOF (Volume of Fluid) method was used to  
 208 determine the free surface position (Olsson et al. 2007).

209 For an incompressible fluid the continuity equation is:

$$\frac{\partial U_i}{\partial x_i} + \frac{\partial U_j}{\partial x_j} + \frac{\partial U_w}{\partial x_w} = 0 \quad (1)$$

210 where  $x_i$ ,  $x_j$  and  $x_w$  are the directions of the cartesian reference coordinate  
 211 system. The generic  $U_y = \frac{1}{T} \int_t^{t+T} u_y dt$  is the time averaged velocity (see eq.  
 212 2) in  $x_y$  direction, where  $u_y$  is the instantaneous flow velocity,  $t$  is the time  
 213 and  $T$  is the integration time interval ( $y$  can be  $i$ ,  $j$  or  $w$ ). In an analogous  
 214 way,  $P = \frac{1}{T} \int_t^{t+T} p dt$ , with  $p$  the instantaneous pressure.

215 The momentum equation in direction  $x_i$ , is:

$$\rho \left( \frac{\partial U_i}{\partial t} + U_i \frac{\partial U_i}{\partial x_i} + U_j \frac{\partial U_i}{\partial x_j} + U_w \frac{\partial U_i}{\partial x_w} \right) = \rho g_i - \frac{\partial P}{\partial x_i} + \mu \nabla^2 U_i + \frac{\partial \tau_{i,i}}{\partial x_i} + \frac{\partial \tau_{i,j}}{\partial x_j} + \frac{\partial \tau_{i,w}}{\partial x_w} \quad (2)$$

216 where  $\rho$  and  $\mu$  are density and dynamic viscosity of the fluid,  $g$  is the  
 217 gravitational acceleration,  $P$  is the time averaged pressure and  $U_i$  is the time  
 218 averaged velocity of the mixture along direction  $x_i$ . Analogous momentum  
 219 equations are solved along directions  $x_j$  and  $x_w$ . The absolute flow velocity

220 is  $U = \sqrt{U_i^2 + U_j^2 + U_w^2}$ .

221 The terms  $\tau_{i,j}$  are the Reynolds turbulent stresses ( $RS$ ), and they can  
222 be expressed as:

$$\tau_{i,j} = -\overline{\rho u'_i u'_j} = \mu_t \left( \frac{\partial U_i}{\partial x_j} + \frac{\partial U_j}{\partial x_i} \right) - \frac{2}{3} \rho k \delta_{ij} \quad (3)$$

223 where  $\mu_t$  is the turbulent dynamic viscosity,  $k$  is the turbulent kinetic energy  
224 and  $\delta_{ij}$  is the Kronecker delta. The fluctuating component  $u'_i$  of velocity in  
225 direction  $i$  is the difference between the instantaneous value of velocity and  
226 the average velocity  $U_i$ .

227 The turbulent dynamic viscosity is calculated using the  $k - \epsilon$  model,  
228 where the turbulent viscosity is expressed as a function of turbulent kinetic  
229 energy  $k$  and turbulent dissipation  $\epsilon$ .

$$\mu_t = \rho C_\mu \frac{k^2}{\epsilon} \quad (4)$$

230 where  $C_\mu = 0.09$ .

231 Turbulent kinetic energy is defined as  $TKE = 1/2[u_i'^2 + u_j'^2 + u_w'^2]$ .

232 The pressure-velocity coupling was solved by PISO (Pressure Implicit  
233 with Splitting of Operator) scheme. Spatial discretizations were realized  
234 by the following schemes: PRESTO for pressure and QUICK for momen-  
235 tum and turbulent kinetic energy, in alignment with Barton et al. (2008).  
236 The Curvature correction was added to sensitize the model to streamline  
237 curvatures. The numerical simulations were run in stationary conditions.  
238 This numerical model has been successfully used in Quaranta et al. (2016),  
239 using a bed slope of 10% and flow rate of 1.20 m<sup>3</sup>/s.

240 When analyzing the results (section 3), average values of flow velocity,  
 241  $TKE$  and  $RS$  in the jet and in resting areas were evaluated. Considering  
 242 flow velocity, the average values were calculated as  $\overline{U_s} = \frac{1}{S_{sides}} \sum^{S_{side}} U dS$   
 243 and  $\overline{U_{jet}} = \frac{1}{S_{jet}} \sum^{S_{jet}} U dS$ , where  $U$  is the time average flow velocity,  $dS$  is  
 244 the infinitesimal area (in this case it is the area of each cell of the mesh)  $S_{side}$   
 245 is the area of the pool side and  $S_{jet}$  is the area of the jet. In an analogous  
 246 way, this process was applied to  $TKE$  and  $RS$  in addition to  $U$ .

#### 247 2.4.1. Boundary conditions

248 At the water inlet, a fixed value of turbulence intensity  $I = \frac{\sqrt{u_i'^2 + u_j'^2 + u_w'^2}}{U} =$   
 249 0.05, with  $U$  the average flow velocity, and a fixed value of turbulent vis-  
 250 cosity ratio  $\mu_t/\mu = 10$  were specified, where  $\mu_t$  is the turbulent dynamic  
 251 viscosity and  $\mu$  is the water dynamic viscosity. This intensity is considered  
 252 a common value used in such type of simulations (Quaranta and Revelli,  
 253 2016), and higher values do not affect the flow field (Marriner et al., 2014).  
 254 The flow rate was imposed at the inlet, as previously described. At the wa-  
 255 ter outlet a fixed water depth was provided in order to ensure the required  
 256  $y_0$  ( $y_0 = 1.0$  m,  $y_0 = 1.5$  m,  $y_0 = 2.0$  m).

### 257 3. Results

258 Planes parallel to the bed were used for the description of the flow field.  
 259 In the following sections, reference will be made predominantly to planes  
 260  $H_2$  and  $H_4$ , since these planes can be considered the most representative  
 261 locations for analyzing the flow field.

262 *3.1. Topology of the flow field*

263 The results obtained in this study for a bed slope of 5% showed that  
264 the flow field was characterized by a main water jet between the slots, with  
265 the generation of one eddy on the right and one eddy on the left side of the  
266 pool. Due to the orientation of the slot ( $\alpha$  in Fig.1), the jet was not straight,  
267 but curved toward the left side of the pool. Furthermore, in Design 16 a  
268 small eddy was generated on the right side of the upstream pointed baffle  
269 (see Figs. 2, 3, 4). The capability of the model to capture this small eddy  
270 confirmed its good performance. Figures 2, 3, 4 show the velocity flow field  
271 of Design 1 and Design 16 for the three water depth values, and along the  
272 investigated planes.

273 In Design 1 the jet exited from the slot at an angle of  $45^\circ$ . Its orientation  
274 with respect to the longitudinal direction after the slots became  $29^\circ$ , due to  
275 its curved shape, and then it was quite straight toward the downstream slot.  
276 This shape was practically constant along the vertical direction. The most  
277 appreciable 3D characteristic was that maximum jet velocity decreased as  
278 it approached the free surface, and jet width became slightly larger.

279 Considering Design 16, the hydraulics were similar to Design 1. How-  
280 ever, in this case the jet between the slots was more curved,  $36^\circ$  vs  $29^\circ$ ,  
281 just downstream of the slot, due to the different slot orientation, and this  
282 characteristic generated significant differences between the two designs.

283 The first effect (a) is that the length of the water jet was longer in  
284 Design 16 ( $l \simeq 1.2L$ ) than the length of the jet in Design 1 ( $l \simeq 1.1L$ ).  
285 Furthermore, (b) in Design 1 the right eddy was more elongated in the  
286 longitudinal direction, while in Design 16 the shape of the eddy on the right

287 approached a more circular shape. The most important consequence (c)  
288 attributed to the larger jet orientation angle in Design 16 was the splitting of  
289 the eddy on the left of the pool into two smaller ones, for all the investigated  
290 flow rates. The last effect (d) is that the jet in Design 16 affected the left  
291 side of the pool (the left side was larger than the right side) more than in  
292 Design 1, reducing the width of resting zones.

### 293 3.2. Flow velocity of jet and resting areas

294 Table 1 reports for each design and flow rate (as well as  $y_0$ ), the max-  
295 imum flow velocity  $U_{max}$  (that occurred in the jet just downstream of the  
296 slot), the average velocity at pool sides ( $\overline{U}_s$ , i.e. the average flow velocity of  
297 areas located outside the main jet) and along the jet ( $\overline{U}_{jet}$ ). The percentage  
298 of pool area  $A$  where the flow velocity in the cell of the mesh was lower than  
299 0.3 m/s, was quantified.

300 With regards to the jet, maximum velocity ( $U_{max}$ ) and average jet ve-  
301 locity ( $\overline{U}_{jet}$ ) decreased as flow rate increased (hence with  $y_0$  increase).

302 In both designs, maximum flow velocity  $U_{max}$  decreased approaching the  
303 free surface; maximum flow velocity on  $H_4$  was about 5.7% (Design 1) and  
304 6.5% (Design 16) lower than maximum flow velocity on  $H_2$  (the width of  
305 the jet spread approaching the free surface). This was valid when  $y_0 = 1$   
306 m and  $y_0 = 1.5$  m, while when  $y_0 = 2$  m maximum flow velocity decrease  
307 was only about 1%. In both designs,  $U_{max}$  decreased of 7-13% (Design 1)  
308 and 2-3% (Design 16) passing from  $y_0 = 1$  m to  $y_0 = 1.5 - 2$  m (hence by  
309 increasing flow rate), on both planes.

310 In Design 1, the decrease of  $u_{jet}$  was 4-10% passing from  $y_0 = 1$  m to  
311  $y_0 = 1.5 - 2$  m on  $H_2$ , but 3-6% when considering the decrease of  $u_{jet}$  with

312  $y_0$  on  $H_4$ . When considering Design 16, the decrease of  $u_{jet}$  was 4-13%  
313 passing from  $y_0 = 1$  m to  $y_0 = 1.5 - 2$  m on  $H_2$ , and it was negligible on  
314  $H_4$ .

315 Average flow velocity in the resting areas ( $\overline{U}_s$ ) reduced when the free  
316 surface was approached;  $\overline{U}_s$  on  $H_4$  was lower than on  $H_2$  of 9-15%. On  $H_2$ ,  
317  $\overline{U}_s$  increased with flow rate (as well as  $y_0$ ); the increase was 10% for Design  
318 1, but for Design 16 no specific trend was identified.

319 Comparing the two designs, maximum velocity magnitude was lower in  
320 Design 16 with respect to Design 1. The difference was about 12% for  $y_0 = 1$   
321 m and about 3% for  $y_0 = 2$  m. Average jet velocity was lower in Design 16  
322 of about 1-5% on  $H_2$ , and 8-11% on  $H_4$ . Instead,  $\overline{U}_s$  was appreciably higher  
323 in Design 16 of more than 16% with respect to Design 1, except for  $y_0 = 2$   
324 m, whose differences were negligible.

325 The area percentage  $A$  remained substantially constant in Design 1 (at  
326 different  $y_0$  and depths), while it was more variable in Design 16, due to  
327 the more variable flow field (vortex splitting). The area  $A$  was generally  
328 wider in Design 1, as it can be observed from Table 1. On the other hand,  
329 on the plane  $H_4$  for  $y_0 > 1$  m,  $A$  was wider in Design 16, and in this case  
330 the differences were more appreciable (11%, which corresponded to 0.7 m<sup>2</sup>,  
331 Table 1). Under these conditions, the vortex splitting almost disappeared,  
332 while a larger vortex appeared instead of two smaller and faster eddies,  
333 contributing to a global decrease of velocity. The resting areas  $A$  were  
334 restricted to between 30% and 50% of the pool.

335 *3.3. Eddy shape and dimensions*

336 With regards to eddy shape and dimensions, the two designs exhibited  
337 different behavior. The jet angle  $\alpha$  (Fig.1) was  $7^\circ$  smaller in Design 16,  
338 leading to a jet more inclined toward the left side of the pool (Fig.1). The  
339 eddy on the left was more elliptical, while the eddy on the right tended  
340 to approach a circular shape. This can be observed in Figs. 2, 3, 4. As  
341 previously described, this eddy on the left under some conditions split into  
342 two smaller ones.

343 Since jet orientation increased slightly with the vertical coordinate, the  
344 vortex splitting occurred in the uppermost part of the pool, and therefore  
345 the flow behavior moved from 2D to 3D in Design 16 (Fig.5). This again  
346 shifts the design choice to Design 1. The jet orientation reduced slightly  
347 with increasing flow rate (i.e.  $y_0$ ); therefore, the higher the flow rate, the  
348 less developed was the vortex splitting. This can be observed looking at  
349 Figs. 2, 3, 4; in Fig. 2, the vortex splitting was well developed, while it was  
350 not in Fig.4, where the flow rate is higher. As a consequence, the minimum  
351 relative depth  $y/y_0$  from which the vortex splitting began, increased with  
352 the increase in flow rate. When  $y_0 = 1.0$  m two eddies were already gen-  
353 erated at  $y/y_0 = 0.33$ ; when  $y_0 = 1.5$  m the presence of two eddies started  
354 at  $y/y_0 = 0.5$ , and the vortex splitting occurred only near the free surface  
355 when  $y_0 = 2.0$  m. A representative case of eddy splitting can be seen in  
356 Fig.5, where the flow field is reported at different planes.

357 All the eddies presented a core zone, with very low velocity (lower than  
358  $0.1$  m/s), and a swirling flow around the rotating core. Table 2 shows the  
359 maximum and minimum dimensions of each eddy core. Where the eddy

360 splitting occurred, the smallest eddy is considered.

361 For Design 1, the maximum eddy dimension, generally along the longi-  
362 tudinal direction, was usually more than twice the smaller one. On the left  
363 side of the pool, the longitudinal eddy dimension was 0.75-1.05 m, while  
364 the transversal one was 0.27-0.54 m. On the right side, dimensions were  
365 0.42-0.71 m in the longitudinal direction and 0.16-0.21 m in the transversal  
366 one.

367 Eddy dimensions slightly reduced as the free surface was approached.  
368 This can be seen in Table 2, comparing for each  $y_0$  longitudinal and transver-  
369 sal eddy dimensions on plane  $H_2$  and  $H_4$ . The difference was generally less  
370 than 10% with respect to the average dimension (the average dimension  
371 was the average between the dimension measured on plane  $H_2$  and  $H_4$ ).

372 Considering Design 16, due to the eddy splitting, the core of eddies was  
373 smaller. On the left side of the pool, the longitudinal eddy dimension was  
374 0.52-0.90 m, while the transversal one was 0.22-0.42 m. On the right side,  
375 dimensions were 0.33-0.69 m in the longitudinal direction and 0.22-0.38 m in  
376 the transversal one. Furthermore, left eddy maximum dimension enlarged  
377 with increasing  $y_0$ , since the eddy splitting started at a relative depth  $y/y_0$   
378 closer to the free surface as  $y_0$  increased. This means that the two smaller  
379 eddies progressively disappeared merging into one bigger vortex.

### 380 3.4. *Turbulent kinetic energy in the pools*

381 Figure 6 depicts an overview of  $TKE$  characteristics in each design,  
382 which is also representative for  $RS$ : the jet was more straight in Design  
383 1, while in Design 16 it was more curved and larger. This distribution  
384 remained qualitatively similar throughout the water column.

385 Table 3 illustrates maximum  $TKE$  ( $TKE_{max}$ ), average  $TKE$  of the jet  
 386 ( $\overline{TKE_{jet}}$ ) and in the pool sides ( $\overline{TKE_s}$ ); the percentage of pool area where  
 387  $TKE \leq 0.05 \text{ m}^2/\text{s}^2$  was also reported. The square root of pool average  
 388  $\overline{TKE}$  was normalized using maximum pool velocity as a scale to obtain a  
 389 dimensionless result.

390 In Design 1  $TKE_{max}$  reduced with increasing water depth  $y_0$  (i.e the  
 391 flow rate) of about 10-35% on  $H_2$ , and 2-5% on  $H_4$ , due to the decrease  
 392 in maximum flow velocity. Maximum  $TKE$  decreased by 15% as the free  
 393 surface was approached, due to the slower jet velocity. In Design 16 a  
 394 monotonic behavior was not easily identified, although maximum  $TKE$   
 395 generally decreased as the free surface was approached and increased by  
 396 increasing flow rate.

397  $\overline{TKE_{jet}}$  increased with the increase in flow rate (passing from  $y_0 = 1$  to  
 398  $y_0 = 1.5 - 2 \text{ m}$ ) of about 4-15% (Design 1) and around 20% (Design 16),  
 399 due to the more intensive turbulence. Average jet velocity was appreciably  
 400 higher on  $H_4$  with respect to  $H_2$ , with an increase of 9-25% for Design 1  
 401 and 10-13% for Design 16 from  $H_2$  to  $H_4$ .

402  $\overline{TKE_s}$  reduced of 9-26% with flow rate in Design 1, while in Design 16  
 403 the decrease was only appreciable on  $H_4$ , and it corresponded to a decrease  
 404 of 8-17% passing from  $y_0 = 1 \text{ m}$  to  $y_0 = 1.5 - 2 \text{ m}$ .  $\overline{TKE_s}$  increased passing  
 405 from  $H_2$  to  $H_4$  (thus it varied with  $y$ ) in Design 1, while it decreased for  
 406 Design 16 (1-17% of decrease). The increasing/decreasing trend with  $y$   
 407 was due to the superimposition of two effects: the enlarging of the jet  
 408 that tended to enhance  $\overline{TKE_s}$ , and the reduction of jet velocity that was  
 409 perceived as a reduction in  $\overline{TKE_s}$ , since the jet had less energy to affect

410 the sides of the pool. These behaviors can be observed in Figs. 2, 3, 4.  
 411 Hence, the final result depended on which effect was predominant. As a  
 412 consequence, average  $TKE$  in the resting zones of the pool was lower in  
 413 Design 1 considering the lowest portion of the pool, but generally higher  
 414 when considering the uppermost portion of the pool.

415 Normalized  $TKE$  was appreciably lower for Design 1. This was con-  
 416 firmed by analyzing the area percentage with  $TKE$  less than  $0.05 \text{ m}^2/\text{s}^2$ :  
 417 it was higher in Design 1, except for  $y_0 = 2 \text{ m}$ .

418 Comparing the two designs, it was possible to observe that the peaks  
 419 of  $TKE$  ( $TKE_{max}$  was in the proximity of the slot) were lower in Design  
 420 16 (due to lower flow velocity) of 13-37%.  $TKE_{jet}$  was higher in Design  
 421 16 on  $H_2$  of 4-24%, but slower on  $H_4$  of 5-10%. A similar behavior can  
 422 be observed for  $TKE_s$ . In Design 16  $TKE_s$  was noticeably higher when  
 423 considering  $H_2$  (12-50% bigger), and only 3-9% lower on  $H_4$  with respect  
 424 to Design 1. The extension of resting zones (where  $TKE \leq 0.05 \text{ m}^2/\text{s}^2$ ) in  
 425 Design 16 was lower by about 2-10% than in Design 1, except when  $y_0 = 2$   
 426 m (8-10% wider). Anyway, low  $TKE$  areas were in both cases wider than  
 427 30% of the pool area, consisting of 39% to 55% of the pool area for Design  
 428 1 and between 35% to 41% for Design 16.

### 429 3.5. Reynolds stresses in the pools

430 Table 4 illustrates maximum  $RS$  ( $RS_{xy,max}$ ), and average jet ( $\overline{RS_{xy,jet}}$ )  
 431 and pool sides ( $\overline{RS_{xy,s}}$ )  $RS$ . The area percentage with  $RS$  in each cell  $\leq 60$   
 432  $\text{N}/\text{m}^2$  is also reported.

433 Maximum  $RS$  increased with flow rate; this was especially observed in  
 434 Design 16, with an increase of more than 31% passing from  $y_0 = 1 \text{ m}$  to

435  $y_0 = 1.5 - 2$  m.  $RS$  decreased approaching the free surface, except for  
436  $y_0 = 2$  m; this again occurred especially for Design 16. The jet average  
437  $RS$  generally increased with flow rate by more than 30% with respect to  
438 the reference situation at  $y_0 = 1$  m.  $RS$  increased as the free surface was  
439 approached.

440 The average  $RS$  in the resting zone was particularly affected by the  
441 flow rate when considering  $H_2$ . It increased when the free surface was  
442 approached, and this occurred especially for Design 1, with increases of  
443 more than 40%. The percentage area where  $RS \leq 60$  N/m<sup>2</sup> was similar for  
444 all designs and conditions; it consisted of 89-97% of the pool area in Design  
445 1 and between 91-97% of pool area in Design 16.

446 As for  $TKE$ , maximum  $RS$  and jet average  $RS$  occurred in Design 1.  
447 Indeed, in Design 1, maximum and average  $RS$  were between 225-283 N/m<sup>2</sup>  
448 and 42-96 N/m<sup>2</sup>, respectively, while in Design 16  $RS$  values were between  
449 110-256 N/m<sup>2</sup> and 37-95 N/m<sup>2</sup>, respectively. Average  $RS_s$  were lower in  
450 Design 1, when considering the lowest portion of the pool, but higher when  
451 considering the uppermost one.

#### 452 4. Discussion

453 Vertical slot fishways are considered the most efficient and least selective  
454 type of technical fishway solutions, and different designs exist. In this study  
455 the two most used designs were investigated (Design 1 and 16), with the  
456 aim of understanding with more details the flow field faced by fish. As  
457 reported in the Introduction, in VSF it is recommended that resting zones  
458 with  $TKE \leq 0.05$  m<sup>2</sup>/s<sup>2</sup> and  $RS \leq 60$  N/m<sup>2</sup> be provided in 30% to 50%

459 of the pool, with velocities kept under 0.30 m/s. Eddies dimensions should  
460 be kept to adequate values compared to upstream migrants body lengths  
461 (Silva et al. 2012; Silva et al., 2015; Marriner et al., 2016).

462 The results achieved in this work were obtained by numerical simula-  
463 tions. The used numerical model was validated in Quaranta et al. (2016)  
464 based on results presented in Rajaratnam et al. (1992). In Quaranta et  
465 al. (2016), the CFD model was applied to Design 1 and 16 for a 10% bed  
466 slope setup, finding a good agreement between experiments and numerical  
467 results. The results presented here are also in good agreement with Khan  
468 (2006), Puertas et al. (2012) and Tarrade et al. (2008). In the follow-  
469 ing paragraphs, comparisons with existing literature and brief resumes of  
470 results will be discussed, with a focus on fish swimming performance.

471 The flow field was characterized by a main water jet between the slots,  
472 curved toward the left side of the pool. With regards to the jet, maximum  
473 velocity ( $U_{max}$ ) and average jet velocity ( $\overline{U_{jet}}$ ) decreased as flow rate in-  
474 creased (hence with  $y_0$  increase). Hence an increase in flow rate is mostly  
475 seen as an increase in water level rather than in velocity, as confirmed by  
476 the equations relating the flow rate  $Q$  with  $y_0$  (Rajaratnam et al., 1992).

477 The jet inclination at the slot was  $29^\circ$  (Design 1) and  $36^\circ$  (Design 16),  
478 due to the different slot geometry. Therefore, in Design 16 the jet between  
479 the slots was more curved, as also shown in Puertas et al. (2012). In Design  
480 1 the jet was not only straighter, but also faster: the faster jet improves the  
481 identification of the upstream path by fish, while it may increase fish energy  
482 expenditure somewhat. In both designs it could be observed the decrease  
483 of maximum jet velocity, with increase in jet width, as the free surface was

484 approached. This 3D effect has been also found by Khan (2006), and it can  
485 be considered the only 3D behavior of Design 1.

486 The curved configuration of the jet generated one eddy on the right and  
487 one eddy on the left side of the pool, each with a central core of lower veloci-  
488 ties. The vortex core may potentially represent a trap for smaller migratory  
489 fish (Silva et al., 2012). Furthermore, due to the higher jet orientation, in  
490 Design 16 the eddy on the right approached a more circular shape and the  
491 jet affected the left side of the pool (which is larger than the right side)  
492 more than in Design 1, reducing the width of resting zones, that fish use  
493 for their rest.

494 In the flow field of Design 16, one further 3D characteristic was found,  
495 in addition to the enlargement of the jet approaching the free surface: the  
496 vortex splitting on the left side of the pool. From a certain water depth,  
497 two smaller eddies were generated from the splitting of the bigger one.  
498 Such smaller eddies are deemed to negatively affect fish behavior, since it  
499 generates two smaller eddies, more comparable with fish dimensions, and  
500 may disorientate them (Silva et al., 2012). Indeed, the transversal eddies  
501 dimension was 0.22-0.42 m, very detrimental especially for fish 0.15-0.40 m  
502 long.

503 In Tarrade et al. (2008) the vortex splitting has been shown also to  
504 occur in Design 1 at 10% slope, as also found in Quaranta et al. (2016),  
505 where the same numerical model here used was applied to Design 1 at 10%  
506 slope.

507 Areas  $A$  with velocities lower than 0.3 m/s (as suggested by Marriner  
508 et al., 2016) were generally wider in Design 1, as it can be observed from

509 Table 1. This aspect is of high importance, especially when considering  
510 the need of resting by fish, after their use of burst speed.  $A$  remained  
511 substantially constant in Design 1, while it was more variable in Design 16,  
512 due to the more variable flow field (vortex splitting). The explanation may  
513 be identified in the superimposition of two effects. The first effect is that  
514 the jet had lower velocity in Design 16, contributing to an increase in low  
515 velocity area percentage  $A$  and a decrease in  $\overline{U_s}$ . Meanwhile, the jet was  
516 more curved (second effect), affecting the sides of the pool more than in  
517 Design 1. The latter effect contributed to the increase in flow velocity and  
518 turbulence at the sides of the pool, and thus to the decrease in areas  $A$ .

519 Maximum and average values of velocity and turbulent variables occur-  
520 ring in the jet were higher when considering Design 1. This means that fish  
521 can locally encounter more fatigue in swimming from one pool to the up-  
522 stream one. However, because of the local validity of the maximum values,  
523 in order to draw more significant conclusions, the average jet values should  
524 be considered when dealing with the burst speed.

525 Considering average water velocities in resting zones, Design 1 is to be  
526 preferred, since resting areas are more quiet. Therefore, in the pool side  
527 fish have the possibility to rest more appropriately, with less fatigue and  
528 using lower prolonged speed. Hence fish can recover the energy they lost  
529 previously in the faster jet.

530 Referring to  $RS$ , the hydraulic configurations were very favorable for  
531 fish, since in more than 90% of the pool area  $RS$  values were lower than the  
532 threshold value (60 N/m<sup>2</sup>, Silva et al., 2011). Therefore, referring to  $RS$ ,  
533 both hydraulic configurations were very favorable for fish.

534 Also  $TKE$  values were lower than the threshold one ( $0.05 \text{ m}^2/\text{s}^2$ , Silva et  
535 al., 2012) in more than 30% of the pool for both designs. The localization of  
536 maximum  $TKE$  areas agrees well with Puertas et al. (2004) for Design 16.  
537 Although turbulent variables respected the threshold values, resting areas  
538 of Design 1 were less turbulent on  $H_2$ , and more turbulent on  $H_4$ . Thus,  
539 Design 1 has a very favorable behavior for fish swimming in the bottom  
540 portion of the pool. Furthermore, normalized  $TKE$  was appreciably lower  
541 for Design 1, hence this design has a more dissipative effect, that makes it  
542 more preferable from a fish passage perspective.

543 In conclusion, the results obtained and presented in this work show  
544 that both designs are adequate for fish upstream migration, even if the  
545 larger eddy dimensions and the more uniform flow behavior make Design  
546 1 more suitable for fish. As a consequence, Design 1 is recommended for  
547 engineering practice in relation to low-gradient VSF. It should be used in  
548 grayling-barbel regions, especially for potamodromous species with body  
549 length within the range 15-40 cm.

## 550 **5. Conclusions**

551 Two typical designs of vertical slot fishways were numerically simulated  
552 and investigated, using a bed slope of 5%. Three flow rates, as well as  
553 water depths, were investigated, and the flow field was compared along two  
554 planes. Results were compared with datasets found in literature, and the  
555 agreement was good.

556 Both designs satisfy prescriptions suggested by scientific literature and  
557 practitioners. Low  $TKE$  and velocity areas were in both cases wider than

558 30% of the pool area, as recommended by Marriner et al. (2014). Referring  
559 to Reynolds stresses, hydraulic configurations were very favorable for fish,  
560 since in more than 90% of the pool area  $RS$  values were lower than the  
561 threshold value ( $60 \text{ N/m}^2$ ).

562 However, results showed that the flow behavior inside the pools was dif-  
563 ferent between the two designs. In Design 1 the flow field was qualitatively  
564 2D, whereas in Design 16 it was more 3D, due to the eddy splitting and the  
565 less straightforward jet. The hydraulic characteristics in Design 16 changed  
566 more significantly with the vertical coordinate than in Design 1. Hence  
567 Design 1 should be preferred over Design 16 from an engineering point of  
568 view.

569 When considering the ecological point of view, conclusions can not be  
570 drawn easily. The flow field in the jet was more turbulent and velocities  
571 were faster in Design 1, but resting areas were more developed and quiet,  
572 providing more appropriate space with low velocities for fish to recover fish  
573 energy. Flow velocities in resting areas were appreciably higher in Design  
574 16 of more than 16% with respect to Design 1. This means that fish need  
575 to use a higher burst speed and a lower prolonged speed in resting zones in  
576 Design 1, that were less turbulent and wider. Therefore, fish may encounter  
577 more fatigue in swimming from one pool to the upstream one in Design 1;  
578 meanwhile, they have the possibility to rest in the pool side, so that they  
579 can recover the energy that was lost in swimming in a more turbulent jet.

580 Considering turbulent kinetic energy, Design 1 is more dissipative. In  
581 Design 16  $TKE$  in resting zones was noticeably higher when considering  
582  $H_2$  (12-50% higher), and only 3-9% lower on  $H_4$  with respect to Design 1.

583 The extension of resting zones (where  $TKE \leq 0.05 \text{ m}^2/\text{s}^2$ ) in Design 16  
584 was lower by about 2-10% than in Design 1, except when  $y_0 = 2 \text{ m}$  (8-10%  
585 wider).

586 As a consequence, it is reasonable to conclude that Design 1, even if 10-  
587 15% more expensive than Design 16 in terms of construction costs, generally  
588 should be considered the recommended design in relation to low-gradient  
589 VSF. This is due to its limited selectivity especially in grayling-barbel re-  
590 gions for potamodromous species with body length within the range 15-40  
591 cm.

## 6. Bibliography

Barton, A., Keller, R., and Katopodis, C. 2008. A free surface model of a vertical slot fishway to numerically predict velocity and turbulence distributions. *American Fisheries Society Symposium*, **61**, 1-16.

Bunt, C. M., Castro-Santos, T., and Haro, A. 2012. Performance of fish passage structures at upstream barriers to migration. *River Research and Applications*, **28**, 457-478.

Calles, E.O. and Greenberg, L.A. 2009. Connectivity is a two-way street – the need for a holistic approach to fish passage problems in regulated rivers. *River Research and Applications*, **25**, 1268-1286.

Clay, C.H. 1995. Design of fishways and other fish facilities. *Second ed.* Lewis Publishers, Boca Raton.

Food and Agriculture Organization of the United Nations (FAO)

Deutscher Verband für Wasserwirtschaft und Kulturbau (DVWK). 2002. Fish passes – design, dimensions and monitoring. *Rome, FAO*.

Hatry, C., Binder, TR., Thiem, JD., Hasler, CT., Smokorowski, KE., Clarke, KD., Katopodis, C., and Cooke, SJ. 2016. The status of fishways in Canada: trends identified using the national canfishpass database. *Rev. Fish Biol. Fish.*, **23**, 271-281.

Heimerl, S., Hagemeyer, M., and Ehteler, C. 2008. Numerical flow simulation of pool-type fishways: new ways with well-known tools. *Hydrobiologia*, **609**, 189-196.

Katopodis, C. 1992. Introduction to fishway design.

Katopodis, C. and Gervais, R. 2016. Fish swimming performance database and analyses. *Fisheries and Oceans Canada*, research document - 2016/002.

Katopodis, C. and Williams, J. 2012. The development of fish passage research in a historical context. *Ecological Engineering*, **48**, 8-18.

Khan, L. 2006. A three-dimensional computational fluid dynamics (CFD) model analysis of free surface hydrodynamics and fish passage energetics in a vertical-slot fishway. *North American Journal of Fisheries Management*, **26**, 255-267.

Laine, A., Kamula, R., and Hooli, J. 1998. Fish and lamprey passage in a combined denil and vertical-slot fishway. *Fisheries Management and Ecology*, **5**, 31-44.

Marriner, B.A., Baki, A.B.M., Zhu, D.Z., Cooke, S.J., and Katopodis, C. 2016. The hydraulics of a vertical slot fishway: A case study on the multi-species Vianney-Legendre fishway in Quebec, Canada. *Ecological Engineering*, **90**, 190-202.

Marriner, B.A., Baki, A.B.M., Zhu, D.Z., Thiem, J.D., Cooke, S.J., and Katopodis, C. 2014. Field and numerical assessment of turning pool hydraulics in a vertical slot fishway. *Ecological Engineering*, **63**, 88-101.

Olsson, E., Kreiss, G., and Zahedi, S. 2007. A conservative level set method for two phase flow II. *Journal of computational Physics*, **225(1)**, 785-807.

Plaut, I. 2012. Critical swimming speed: its ecological relevance. *Comparative Biochemistry and Physiology, part A*, **131**, 41-50.

Puertas, J., Cea, L., Bermúdez, M., Pena, L., Rodríguez, A., Rabunal, J.R., Balairón, L., Lara, A., and Aramburu, E. 2012. Computer application for the analysis and design of vertical slot fishways in accordance with the requirements of the target species. *Ecological Engineering*, **48**, 51-60.

Puertas, J., Pena, L., and Teijeiro, T. 2004. Experimental approach to the hydraulics of vertical-slot fishways. *Journal of Hydraulic Engineering*, **130**, 10-23.

Quaranta, E., Comoglio, C., Katopodis, C., and Revelli, R. 2016. Numerical simulations of flow field in vertical slot fishways. *Idra16, XXXV National Congress on Hydraulics and Hydraulic Structures, Bologna, Italy, 14-16 September, 749-752*.

Quaranta, E. and Revelli, R. 2016. Hydraulic behavior and performance of breastshot water wheels for different numbers of blades. *Hydraulic Engineering*, **143** (1), 04016072-1.

Rajaratnam, N., Katopodis, C., and Solanki, S. 1992. New designs for vertical-slot fishways. *Canadian Journal of Civil Engineering*, **19**, 402-414.

Santos, JM., Silva, AT., Katopodis, C., Pinheiro, PJ., Pinheiro, AN., Bochechas, J., and Ferreira, MT. 2016. Ecohydraulics of pool-type fishways: getting past the barriers. *Ecological Engineering*, **48**, 38-50.

Schmutz, S. and Mielach, C. 2013. Measures for ensuring fish migration at transversal structures. *International Commission for the Protection of the Danube River*.

Silva, A., Hatry, C., Thiem, J., Gutowsky, L., Hatin, D., Zhu, D., Dawson, J., Katopodis, C., and Cooke, S. 2015. Behaviour and locomotor activity of a migratory catostomid during fishway passage. *PLoS ONE*, **10**(4): e0123051.

Silva, A., Santos, J., Ferreira, M., Pinheiro, A., and Katopodis, C. 2011. Effects of water velocity and turbulence on the behaviour of Iberian barbel (*luciobarbus bocagei*, Steindachner 1864) in an experimental pool-type fishway. *River Research and Applications*, **27**, 360-373.

Silva, A.T., Katopodis, C., Santos, J.M., Ferreira, M.T., and Pinheiro, A.N. 2012. Cyprinid swimming behaviour in response to turbulent flow. *Ecological Engineering*, **44**, 314-328.

Stuart, I. G. and Berghuis, A. P. 2002. Upstream passage of fish through a vertical-slot fishway in an Australian subtropical river. *Fisheries Management and Ecology*, **9**, 111-122.

Tarrade, L., Texier, A., David, L., and Larinier, M. 2008. Topologies and measurements of turbulent flow in vertical slot fishways. *Hydrobiologia*, **609 (1)**, 177-188.

Tritico, H.M and Cotel, A.J. 2010. The effects of turbulent eddies on the stability and critical swimming speed of creek chub (*semotilus atromaculatus*). *Journal of Experimental Biology*, 2284-2293.

White, L.J., Harris, J.H., and Keller, R.J. 2011. Movement of three non-salmonid fish species through a low-gradient vertical-slot fishway. *River Research and Applications*, **27 (4)**, 499-510.

Wu, S., Rajaratnam, N., and Katopodis, C. 1999. Structure of flow in vertical-slot fishway. *Journal of Hydraulic Engineering*, **125**, 352-360.

## List of Figures

1	Geometric features of Design 1 and Design 16 of VSF (adapted from Rajaratnam et al., 1992). Design 16 differs from Design 1 in the geometry of the baffles, whereas for both designs the pool dimensions are the same. In the CFD model the reference value $b_0 = 0.30$ m was used. . . . .	34
2	Velocity flow field of Design 1 (top) and 16 (bottom) for $y_0 = 1$ m on planes $H_2$ and $H_4$ . Units in m/s. . . . .	35
3	Velocity flow field of Design 1 (top) and 16 (bottom) for $y_0 = 1.5$ m on planes $H_2$ and $H_4$ . Units in m/s. . . . .	36
4	Velocity flow field of Design 1 (top) and 16 (bottom) for $y_0 = 2$ m on planes $H_2$ and $H_4$ . Units in m/s. . . . .	36
5	Velocity flow field of Design 16 for $y_0 = 1$ m on different planes. Units in m/s. . . . .	37
6	Turbulent kinetic energy for Design 1 (top) and Design 16 (bottom) at $y_0 = 1.0, 1.5, 2.0$ m along the representative plane $H_3$ at $y = 0.5y_0$ . The $TKE$ field remains qualitatively similar along the water column. Units in $m^2/s^2$ . . . . .	38

**Table 1.** Maximum flow velocity ( $U_{max}$ ), average flow velocities in the jet ( $\overline{U}_{jet}$ ) and in the area outside the jet ( $\overline{U}_s$ ), and area percentage ( $A$ ) with velocities lower than 0.3 m/s, on the plane  $H_2 = 0.33y_0$  and  $H_4 = 0.67y_0$ . Units are reported.

Plane	$y_0$	$D1$				$D16$			
		$U_{max}$	$\overline{U}_{jet}$	$\overline{U}_s$	$A$	$U_{max}$	$\overline{U}_{jet}$	$\overline{U}_s$	$A$
	m	m/s	m/s	m/s	%	m/s	m/s	m/s	%
$H_2$	1.0	1.91	1.28	0.28	0.43	1.68	1.26	0.33	0.35
	1.5	1.75	1.22	0.31	0.46	1.62	1.21	0.36	0.43
	2.0	1.65	1.15	0.31	0.42	1.62	1.09	0.32	0.41
$H_4$	1.0	1.80	1.16	0.28	0.48	1.56	1.07	0.38	0.47
	1.5	1.65	1.24	0.26	0.46	1.52	1.10	0.31	0.51
	2.0	1.67	1.20	0.28	0.47	1.60	1.07	0.27	0.52

**Table 2.** Maximum and minimum dimensions of each eddy core forming on the left and on the right of the water jet, on the plane  $H_2 = 0.33y_0$  and  $H_4 = 0.67y_0$ . Units are reported.

Plane	$y_0$	$D1$				$D16$			
		left		right		left		right	
	m	$d_{max}$	$d_{min}$	$d_{max}$	$d_{min}$	$d_{max}$	$d_{min}$	$d_{max}$	$d_{min}$
		m	m	m	m	m	m	m	m
$H_2$	1.0	1.05	0.42	0.63	0.21	0.54	0.22	0.54	0.38
	1.5	0.98	0.54	0.71	0.27	0.52	0.29	0.69	0.23
	2.0	0.79	0.42	0.63	0.21	0.90	0.42	0.59	0.30
$H_4$	1.0	0.79	0.37	0.53	0.26	0.67	0.22	0.33	0.22
	1.5	0.74	0.27	0.54	0.22	0.68	0.23	0.51	0.28
	2.0	0.84	0.32	0.42	0.16	0.86	0.34	0.57	0.34

**Table 3.** Maximum  $TKE$  ( $TKE_{max}$ ), jet average  $TKE$  ( $\overline{TKE_{jet}}$ ), pool's sides average  $TKE$  ( $\overline{TKE_s}$ ), dimensionless value of  $TKE$ , and area percentage  $A$  where  $TKE$  is lower than  $0.05 \text{ m}^2/\text{s}^2$ , on the plane  $H_2 = 0.33y_0$  and  $H_4 = 0.67y_0$ . Units are reported.

Plane	$y_0$	D1					D16				
		$TKE_{max}$	$\overline{TKE_{jet}}$	$\overline{TKE_s}$	$\frac{\sqrt{TKE}}{v_{max}}$	$A$	$TKE_m$	$\overline{TKE_{jet}}$	$\overline{TKE_s}$	$\frac{\sqrt{TKE}}{v_{max}}$	$A$
	m	$\text{m}^2/\text{s}^2$	$\text{m}^2/\text{s}^2$	$\text{m}^2/\text{s}^2$	-	%	$\text{m}^2/\text{s}^2$	$\text{m}^2/\text{s}^2$	$\text{m}^2/\text{s}^2$	-	%
$H_2$	1.0	0.40	0.162	0.065	0.159	0.39	0.32	0.169	0.073	0.191	0.35
	1.5	0.36	0.147	0.048	0.147	0.55	0.31	0.154	0.072	0.177	0.40
	2.0	0.26	0.170	0.059	0.160	0.39	0.34	0.211	0.077	0.177	0.42
$H_4$	1.0	0.35	0.177	0.077	0.156	0.43	0.22	0.158	0.072	0.188	0.39
	1.5	0.34	0.198	0.066	0.166	0.45	0.26	0.186	0.060	0.187	0.41
	2.0	0.33	0.204	0.064	0.164	0.41	0.33	0.192	0.066	0.172	0.45

**Table 4.** Maximum Reynolds stresses  $RS_{xy,max}$ , average Reynolds stresses in the jet  $\overline{RS_{xy,jet}}$  and in the pool's sides  $\overline{RS_{xy,s}}$ , and area percentage with  $RS \leq 60 \text{ N/m}^2$ , on the plane  $H_2 = 0.33y_0$  and  $H_4 = 0.67y_0$ . Units are reported.

Plane	$y_0$	D1				D16			
		$RS_{xy,max}$	$\overline{RS_{xy,jet}}$	$\overline{RS_{xy,s}}$	$A$	$RS_{xy,max}$	$\overline{RS_{xy,jet}}$	$\overline{RS_{xy,s}}$	$A$
	m	$\text{N/m}^2$	$\text{N/m}^2$	$\text{N/m}^2$	%	$\text{N/m}^2$	$\text{N/m}^2$	$\text{N/m}^2$	%
$H_2$	1.0	261.4	49.7	11.2	0.91	195.4	40.9	11.8	0.96
	1.5	282.6	41.9	10.0	0.96	192.8	36.6	14.6	0.96
	2.0	259.0	84.6	13.7	0.89	256.4	95.3	16.9	0.97
$H_4$	1.0	224.7	60.0	16.7	0.97	110.8	49.9	12.5	0.94
	1.5	242.5	81.1	17.7	0.96	161.3	74.7	12.0	0.95
	2.0	272.9	96.4	16.6	0.96	246.7	87.7	14.2	0.91

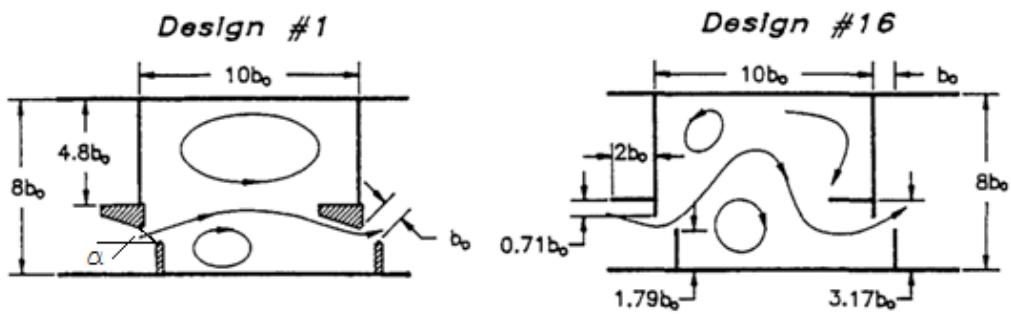


**Fig. 1.** Geometric features of Design 1 and Design 16 of VSF (adapted from Rajaratnam et al., 1992). Design 16 differs from Design 1 in the geometry of the baffles, whereas for both designs the pool dimensions are the same. In the CFD model the reference value  $b_0 = 0.30$  m was used.

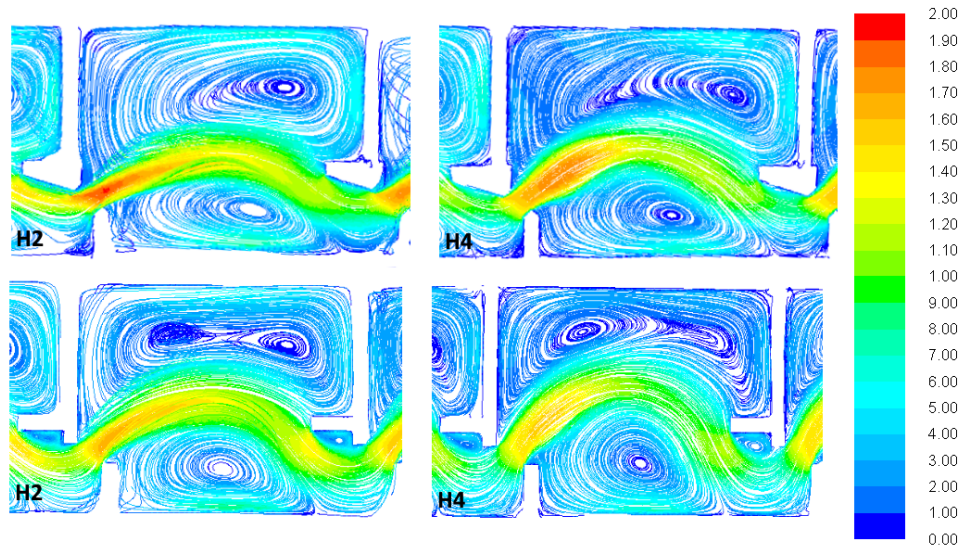


**Fig. 2.** Velocity flow field of Design 1 (top) and 16 (bottom) for  $y_0 = 1$  m on planes  $H_2$  and  $H_4$ . Units in m/s.

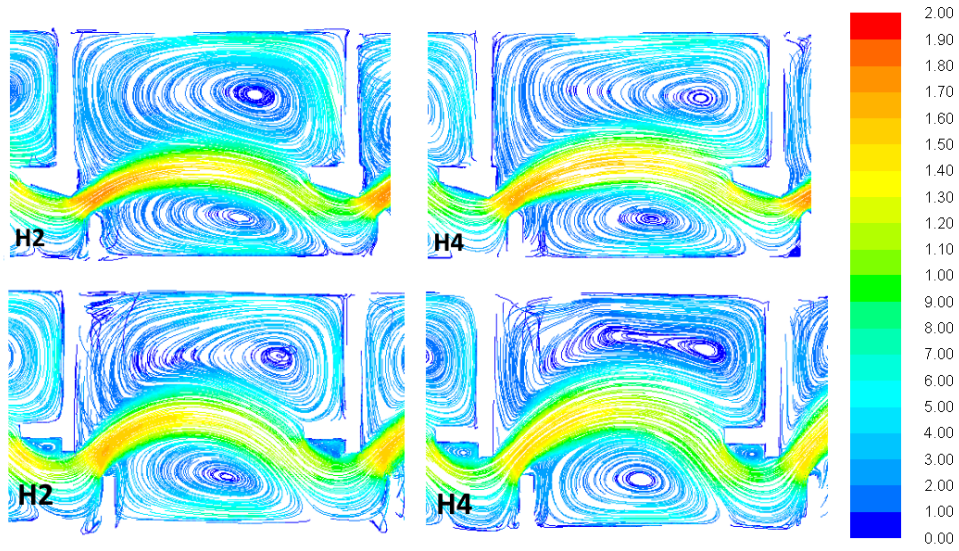


**Fig. 3.** Velocity flow field of Design 1 (top) and 16 (bottom) for  $y_0 = 1.5$  m on planes  $H_2$  and  $H_4$ . Units in m/s.

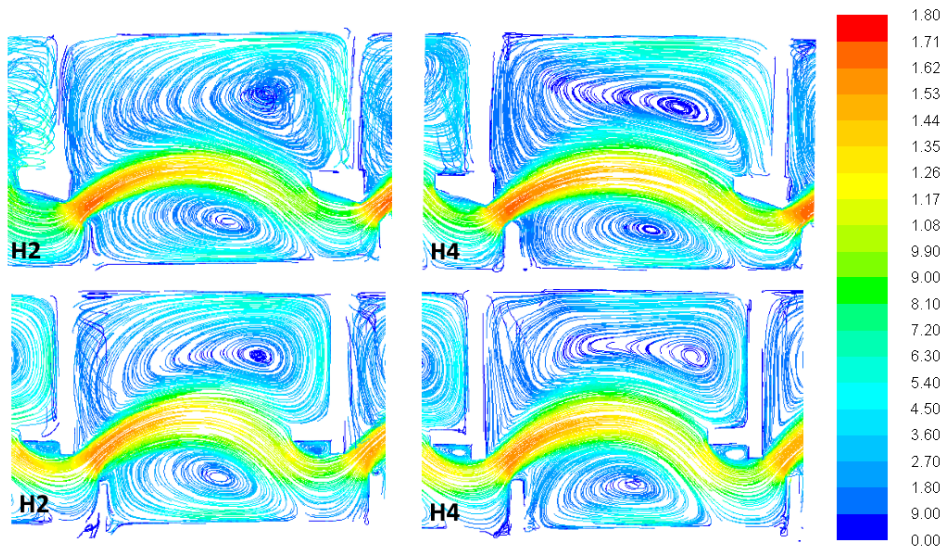


**Fig. 4.** Velocity flow field of Design 1 (top) and 16 (bottom) for  $y_0 = 2$  m on planes  $H_2$  and  $H_4$ . Units in m/s.

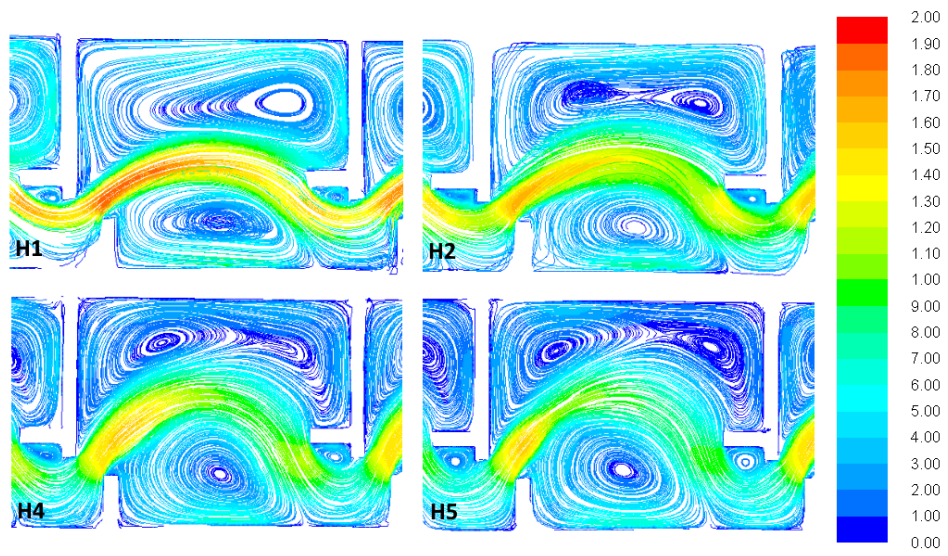


**Fig. 5.** Velocity flow field of Design 16 for  $y_0 = 1$  m on different planes. Units in m/s.

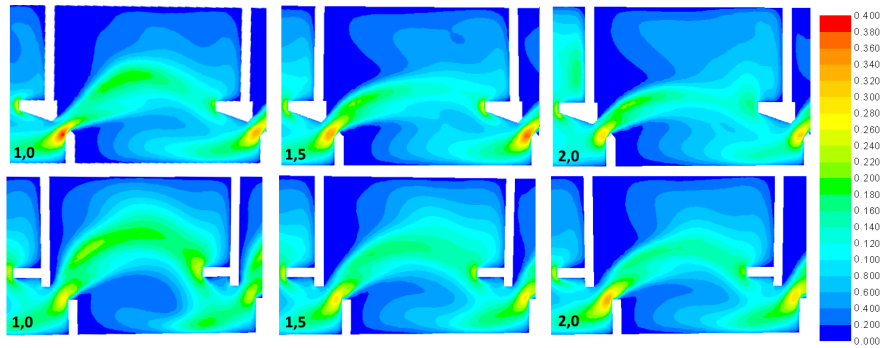


**Fig. 6.** Turbulent kinetic energy for Design 1 (top) and Design 16 (bottom) at  $y_0 = 1.0, 1.5, 2.0$  m along the representative plane  $H_3$  at  $y = 0.5y_0$ . The  $TKE$  field remains qualitatively similar along the water column. Units in  $\text{m}^2/\text{s}^2$ .